J. Fluid Mech. (2003), *vol.* 492, *pp.* 231–250.
DOI: 10.1017/S0022112003005561 Printed in the United Kingdom

Breakup in stochastic Stokes flows: sub-Kolmogorov drops in isotropic turbulence

By VITTORIO CRISTINI[1], J. BŁAWZDZIEWICZ[2], MICHAEL LOEWENBERG[3] AND LANCE R. COLLINS[4]

[1]Department of Biomedical Engineering, University of California, Irvine, CA 92612, USA

[2]Department of Mechanical Engineering, Yale University, New Haven, CT 06520-8286, USA

[3]Department of Chemical Engineering, Yale University, New Haven, CT 06520-8286, USA

[4]School of Mechanical and Aerospace Engineering, Cornell University, Ithaca, NY 14853-7501, USA

(Received 23 September 1998 and in revised form 7 May 2003)

Deformation and breakup of drops in an isotropic turbulent flow has been studied by numerical simulation. The numerical method involves a pseudospectral representation of the turbulent outer flow field coupled to three-dimensional boundary integral simulations of the local drop dynamics. A statistical analysis based on an ensemble of drop trajectories is presented; results include breakup rates, the distribution of primary daughter drops produced by breakup events, and stationary distributions for drop deformation and orientation. Depending on the local flow history, drops may break at modest length or become highly elongated and relax without breaking. Drop deformation is the dominant mechanism of drop reorientation. The volume of the primary daughter drops, produced by a given fluctuation in flow strength, scales with the volume of the corresponding critical drop size for the fluctuation. A simplified description for the evolution of the drop size distribution, based on this scaling, is presented.

1. Introduction

Drop breakup in turbulent flows is relevant to a broad range of engineering applications, including liquid–liquid extraction, emulsification and homogenization processes, spraying, mixing and blending, and multiphase chemical reactors. Process design and scale-up are hampered by the lack of reliable models for the breakup process.

The phenomenological model proposed by Kolmogorov (1949) and Hinze (1955) forms the basis of almost all of the current models for predicting drop breakup in turbulent flows. According to this classical picture, breakup occurs when the distorting hydrodynamic stress associated with a turbulent eddy exceeds the restoring stress of surface tension. The hydrodynamic stress is dominated by inertia for drops that are larger than the Kolmogorov dissipation length and by viscosity for drops that are smaller. For each regime, an estimate is thus obtained for the critical drop size above which breakup will occur in a typical fluctuation.

The population balance equation that describes the evolution of a drop size distribution requires models for the breakup rates of individual drops in a fluctuating flow field, the distribution of daughter drops produced by the breakup of a parent drop, and pairwise coalescence rates (Coulaloglou & Tavlarides 1977; Tsouris & Tavlarides

1994). Most of the recently developed phenomenological models for breakup rates and daughter-drop-size distribution functions are based on the assumption that drops are larger than the Kolmogorov dissipation length. Typically, this regime is relevant to low-viscosity fluids (e.g. water, air) (see the review by Lasheras *et al.* 2002). Detailed simulations for the dynamics of a drop subjected to an axisymmetric pressure disturbance were used by Shreekumar, Kumar & Gandhi (1996) as a model for the drop dynamics in this regime. Ramkrishna and co-workers developed a procedure for extracting breakup rates and daughter-drop-size distribution functions from transient drop-size distribution data by solving the population balance equation as an inverse problem (Sathyagal, Ramkrishna & Narsimhan 1996; Ramkrishna 2000). Their procedure is model-independent aside from the assumption that the volume of daughter drops produced by a breakup event scale with the volume of the parent drop.

The present article describes a numerical study of drop dynamics and breakup for the complementary regime of drops that are smaller than the Kolmogorov dissipation length. Hinze (1955) recognized the relevance of sub-Kolmogorov drop breakup in high-viscosity fluids, but few models have been developed. The problem of computing drop dynamics in the sub-Kolmogorov regime is simplified considerably by the disparity of the relevant lengthscales. Accordingly, the local drop dynamics are described by the Stokes equations in a time-dependent linear flow that matches to the turbulent outer flow. The situation is similar to the problem of drop dynamics in stochastic low-Reynolds-number flows, including mixing flows (Tjahjadi & Ottino 1991) and flows in porous media (Patel *et al.* 2003). Thus, the study presented in this paper is relevant to a broader class of problems involving drop breakup in stochastic flows.

The assumptions in our analysis are given in § 2, and the numerical method is described in § 3. Qualitative features of the drop dynamics are presented in § 4. A statistical analysis of an ensemble of drops is presented in § 5.

2. Assumptions

We consider isotropic homogeneous turbulent flow of a dilute dispersion of deformable drops with constant interfacial tension σ. The dynamic viscosities of the continuous- and drop-phase fluids are μ and $\lambda\mu$. The turbulence is characterized by the Kolmogorov dissipation length

$$\eta = \nu^{3/4}\epsilon^{-1/4}, \tag{2.1}$$

where ϵ is the average energy dissipation rate per unit mass, $\nu = \mu/\rho$ is the kinematic viscosity, and ρ is the mass density of the continuous-phase fluid; the Kolmogorov timescale is $\tau_\eta = \eta^2/\nu$.

Herein, we assume that the drops are small compared to the Kolmogorov scale

$$a/\eta \ll 1, \tag{2.2}$$

where $v = 4\pi a^3/3$ is the drop volume. In this regime, viscous stresses $\Sigma_\mu = \mu/\tau_\eta$ dominate inertial stresses $\Sigma_\rho = \rho a^2/\tau_\eta^2$ at the drop scale because $\Sigma_\rho/\Sigma_\mu = (a/\eta)^2$. Accordingly, the local velocity field in the neighbourhood of a drop is governed by the Stokes equations. The trajectory of the centre-of-mass of a drop nearly coincides with the trajectory of a material element in the turbulent outer flow, provided that the density contrast between the continuous- and drop-phase fluids is moderate (i.e. liquid–liquid dispersion).

For low- and moderate-viscosity ratios, $\lambda \lesssim 1$, the time scale for drop dynamics is set by the capillary relaxation time $\tau_\sigma = \mu a/\sigma$, where σ is the surface tension; for $\lambda \gg 1$, the relevant time scale is $\lambda\tau_\sigma$. Most of the results in this paper correspond to $\lambda = 1$, although a limited set of results for $\lambda = 0.1$ and $\lambda = 5$ is also presented.

The drop-size parameter $\bar{v}$ is defined by the ratio of time scales

$$\bar{v}^{1/3} = \tau_\sigma/\tau_\eta. \tag{2.3}$$

The parameter $\bar{v}$ can be interpreted as the drop volume non-dimensionalized by $4\pi(\sigma\tau_\eta/\mu)^3/3$, and $\bar{v}^{1/3}$ is the capillary number for the system. Drop deformation is significant for $\bar{v} \approx 1$ and breakup occurs for $\bar{v}$ beyond a critical value which depends on the history of the local flow field.

The sub-Kolmogorov regime is defined by (2.2). Taking $\bar{v} \approx 1$, we find

$$a/\eta \sim \mu^{-5/4}\sigma\rho^{1/4}\epsilon^{-1/4}, \tag{2.4}$$

which indicates that sub-Kolmogorov drop breakup may occur in high-viscosity fluids. An example of conditions corresponding to sub-Kolmogorov breakup ($a/\eta = 0.2$, $\bar{v}^{1/3} = 0.3$) is obtained for drops with 10 μm radius in an emulsion with $\mu = \lambda\mu = 20$ cP, $\rho = 1000\,\mathrm{kg\,m^{-3}}$, and $\sigma = 0.005\,\mathrm{N\,m^{-1}}$ in a turbulent flow with an average dissipation rate $\epsilon = 10^3\,\mathrm{W\,kg^{-1}}$.

For systems with an initial drop size distribution larger than the Kolmogorov length, the sub-Kolmogorov regime is achieved at long-times, provided that the right-hand side of (2.4) is small compared to unity.

3. Numerical method

3.1. *Outer turbulent flow*

Under the assumption that the dispersion is dilute, and the density contrast of the fluids is moderate, the turbulent outer flow $\boldsymbol{u}_o$ is unaffected by the presence of the drops. Moreover, trajectories of the drop centre-of-mass $\boldsymbol{x}_c(t)$ can be approximated by the trajectories of material elements,

$$\frac{\mathrm{d}\boldsymbol{x}_c}{\mathrm{d}t} = \boldsymbol{u}_o(\boldsymbol{x}_c, t), \tag{3.1}$$

and pre-calculated. The velocity field $\boldsymbol{u}_o$ was computed by solving the Navier–Stokes equations with periodic boundary conditions, using a pseudospectral method (Canuto *et al.* 1988). Stationary turbulence was maintained by adding energy to the long-wavenumber modes with a random forcing (Eswaran & Pope 1988). Physical space was discretized on a 64^3 lattice, and wavenumbers up to $1.5\eta^{-1}$ were used (Sundaram & Collins 1997). The velocity field between lattice points was obtained by spectral interpolation. The Reynolds number based on the Taylor microscale for this system is 54. Fluctuations of the energy dissipation rate about the mean value are known to increase with Reynolds number (Frisch 1995); however, the Reynolds-number-dependence of the drop dynamics was not explored in our study.

3.2. *Local drop dynamics*

3.2.1. *Boundary integral formulation*

According to the assumptions discussed in § 2, the local velocity field is described by the Stokes equations with boundary conditions appropriate for deformable drops with constant interfacial tension (i.e. velocity and tangential stress continuous at the drop interface, and a normal stress discontinuity resulting from capillary stresses).

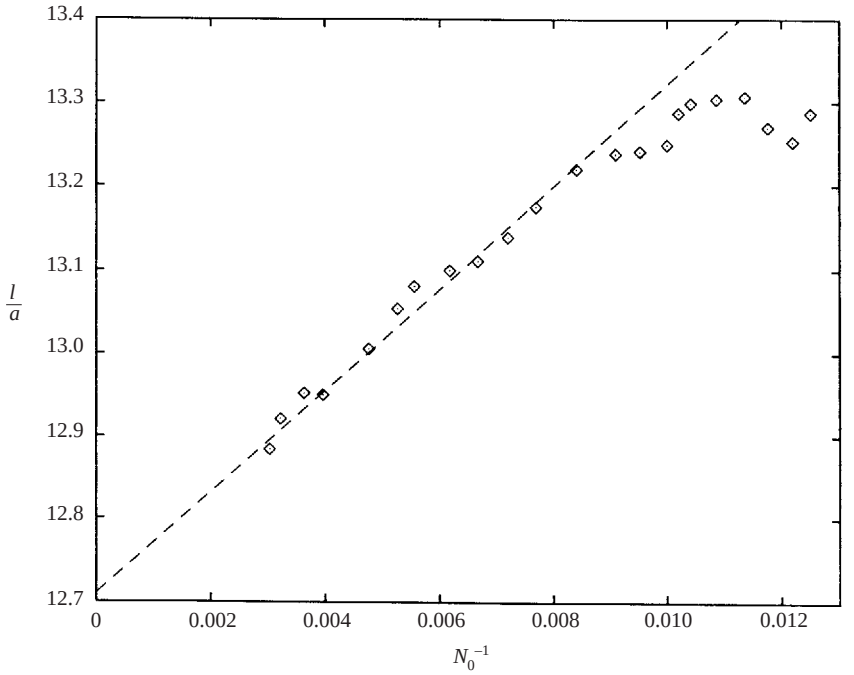

FIGURE 1. Maximum drop length for trajectory (*b*) in figure 2 as a function of mesh resolution N_0^{-1} (points); linear fit (dashed line).

Drop-shape evolution was computed by integrating the the fluid velocity $\boldsymbol{u}(\boldsymbol{x})$ on the drop interface. The velocity field $\boldsymbol{u}(\boldsymbol{x})$ was obtained by solving the boundary integral equation for Stokes flow (Pozrikidis 1992) with a far field that matches to a linear expansion of the turbulent outer flow about the drop trajectory,

$$\boldsymbol{u}^{\infty}(\boldsymbol{x}, t) = (\boldsymbol{x} - \boldsymbol{x}_c) \cdot [\boldsymbol{e}(t) + \boldsymbol{w}(t)]. \tag{3.2}$$

Here, $\boldsymbol{e}(t)$ and $\boldsymbol{w}(t)$ are the symmetric and antisymmetric tensors that describe the straining and rotational components of the flow, respectively.

The boundary integral equation was iteratively solved on a set of N interfacial marker points at each time step of the drop-shape evolution. Between time steps, the discretization of the drop interface was adaptively restructured to maintain uniform resolution of the pointwise curvature with a prescribed accuracy determined by the number of marker points N_0 used to discretize the initial (spherical) drop shape (Cristini, Bławzdziewicz & Loewenberg 2001). Figure 1 shows the maximum drop length attained on trajectory (*b*) in figure 2 as a function of mesh resolution N_0^{-1}. Drop length is defined as the diameter of the sphere that circumscribes the drop shape. The results shown in figure 1 indicate that discretization errors are approximately $O(N_0^{-1})$. The calculations presented in this paper were obtained using $N_0 = 100$, which corresponds to approximately 5% discretization error, according to the figure.

Critical values of the drop-size parameter $\bar{v}^*$ for isolated fluctuations in flow strength along a given trajectory were determined to within 1% accuracy (for a fixed discretization N_0) from a series of simulations. The critical drop length l^*, defined as the maximum length without breakup on a particular fluctuation, was obtained by extrapolating from the maximum lengths achieved for subcritical-size drops. Breakup times at pinch-off t_b and (primary) daughter drop volumes v_d for supercritical-size

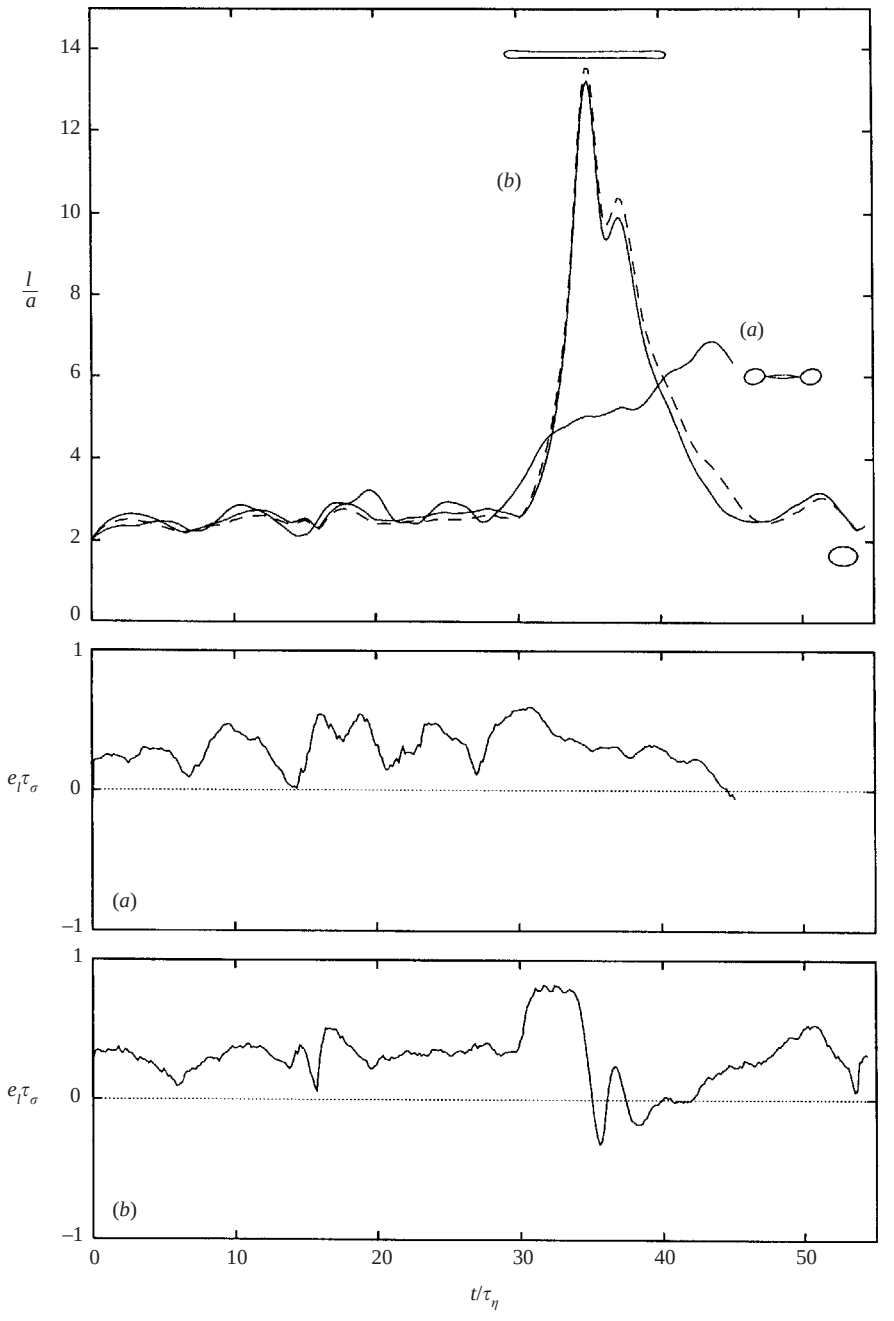

FIGURE 2. Evolution of drop length and projected strain rate on two trajectories, $\bar{v}^{1/3} = 0.3$, $\lambda = 1$ (solid curves). Final drop shapes and shape at maximum length on trajectory (*b*) are shown. Axisymmetric approximation (4.3) corresponding to drop-size parameter $\bar{v}^{1/3} = 0.25$ (dashed curve).

drops were obtained by extrapolating in time to the pinch-off event from simulations that describe the evolution close to pinch-off (Lister & Stone 1998; Bławzdziewicz, Cristini & Loewenberg 1997). Satellite drops produced by the subsequent breakup of the elongated neck region were not resolved in our simulations.

4. Drop trajectories

Qualitative features of drop dynamics are illustrated in this section. The evolution of drop length l for two drop trajectories is shown in figure 2. The strength of the local flow field along the trajectories is characterized by the strain projection

$$e_l = \hat{\boldsymbol{l}} \cdot \mathbf{e} \cdot \hat{\boldsymbol{l}}, \tag{4.1}$$

where $\hat{\boldsymbol{l}}$ is the drop-orientation vector, and $\mathbf{e}$ is the rate-of-strain tensor. Selected drop shapes along the trajectories are shown in figure 3. The point-symmetry of the drop shapes results from the symmetry of the linear incident flow field (3.2) and spherical initial conditions.

The drop on trajectory (a) in figure 2 breaks after moderate elongation ($l/a \approx 7$), while the drop on trajectory (b) becomes much more distorted ($l/a \approx 13$) but relaxes to a nearly spherical shape. The two drops experience qualitatively different projected strain histories, as shown in figure 2. Drop (a) experiences a modest straining fluctuation that decays slowly; the fluctuation stretches the drop and maintains its elongation until a neck forms, as shown in figure 3(a). The neck thins under capillary pressure, and pinch-off occurs. In contrast, drop (b) encounters a larger fluctuation that strongly stretches the drop; however, the straining fluctuation decays rapidly, and is followed by compressional flow ($e_l < 0$). Thus, the drop retracts quickly, and only a shallow neck develops, as seen in figure 3(b). The foregoing example shows that the drop dynamics depend on the detailed history of the local flow field.

On a given trajectory, the drop dynamics depend on the viscosity ratio and drop-size parameter $\bar{v}$. The effects of these parameters are illustrated in figure 4. Here, the strength of the local flow field is characterized by

$$e_{max} = max(e_1, e_2, e_3), \tag{4.2}$$

where (e_1, e_2, e_3) are the eigenvalues of the rate-of-strain tensor $\mathbf{e}$. The results show that for breaking trajectories, the drop length at pinch-off increases approximately linearly with the drop-size parameter $\bar{v}$. This is because the elongation rate after a neck region forms is dominated by the local strain rate, but the neck thinning rate is proportional to surface tension. Subsequent breakup of the elongated neck by end-pinching or the capillary-wave instability would yield several smaller satellite drops; however, this process was not resolved in our simulations.

The results in figure 4 also show that low-viscosity drops (i.e. $\lambda = 0.1$ and $\lambda = 1$) respond quickly to changes in the flow field because $\tau_\sigma \lesssim \tau_\eta$. For high-viscosity drops ($\lambda = 5$), the relevant timescale is comparatively longer $\lambda\tau_\sigma > \tau_\eta$, thus drops respond more slowly and have a longer memory of the flow-field history. The drop length at pinch-off increases with λ for $\lambda \gg 1$, because the neck thinning rate is proportional to λ^{-1}.

We found that qualitative features of the three-dimensional drop dynamics can be predicted using an axisymmetric approximation, provided that the drop-orientation vector $\hat{\boldsymbol{l}}(t)$ is known. According to this approximation, the incident flow field (3.2) is represented by

$$u_z^\infty = e_l z, \qquad u_s^\infty = -\tfrac{1}{2} e_l s, \tag{4.3}$$

where (s, z) are cylindrical coordinates with radial distance s and the z-axis parallel to $\hat{\boldsymbol{l}}$. The corresponding velocity components are $(u_s u_z)$, and e_l is the projected strain (4.1). This approximation was tested on several trajectories by using $\hat{\boldsymbol{l}}(t)$ obtained from our three-dimensional simulations. In all cases, this approximation gave qualitatively

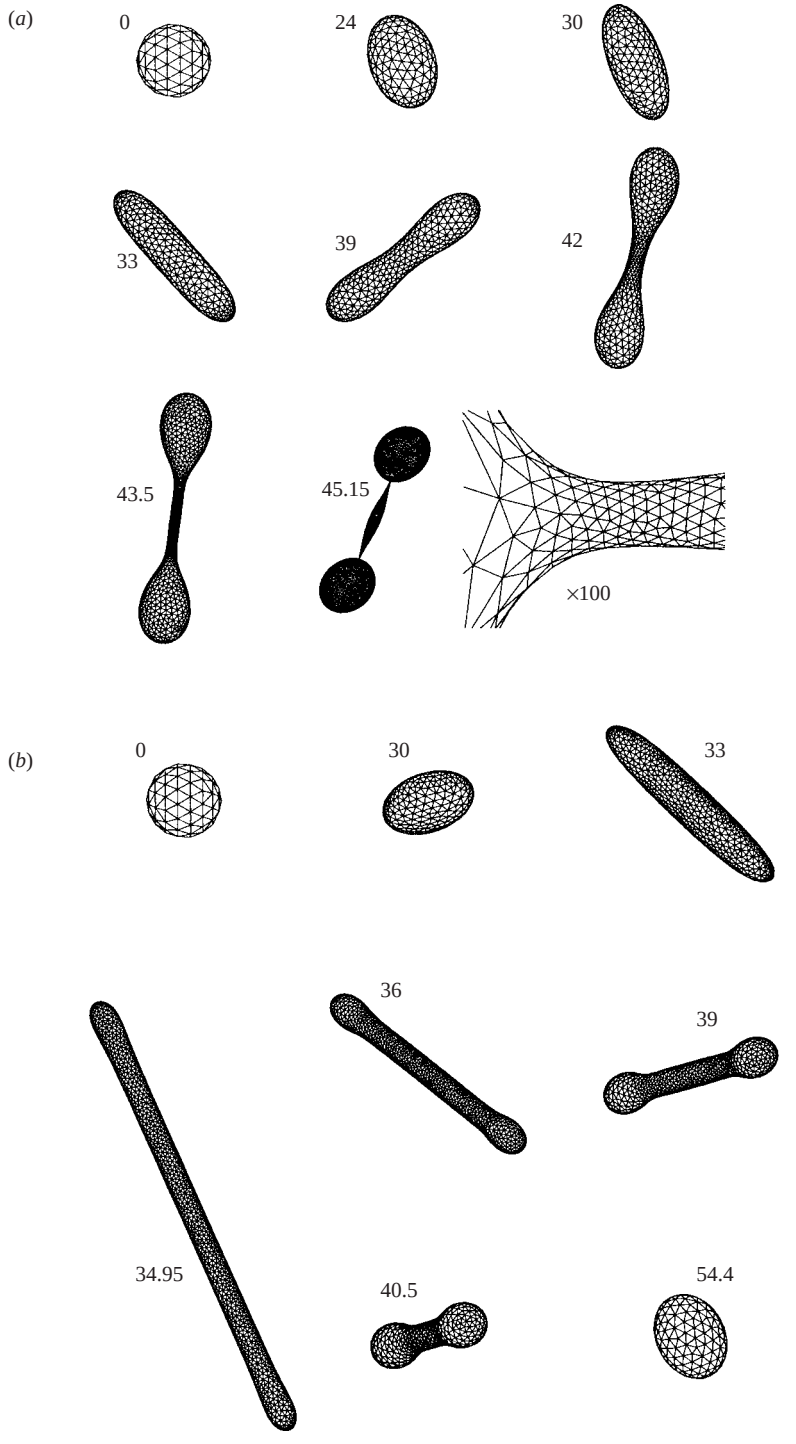

FIGURE 3. Sequence of drop shapes corresponding to trajectories (*a*) and (*b*) in figure 2, at times t/τ_η indicated; inset shows neck region for trajectory (*a*) at $t/\tau_\eta = 45.15$.

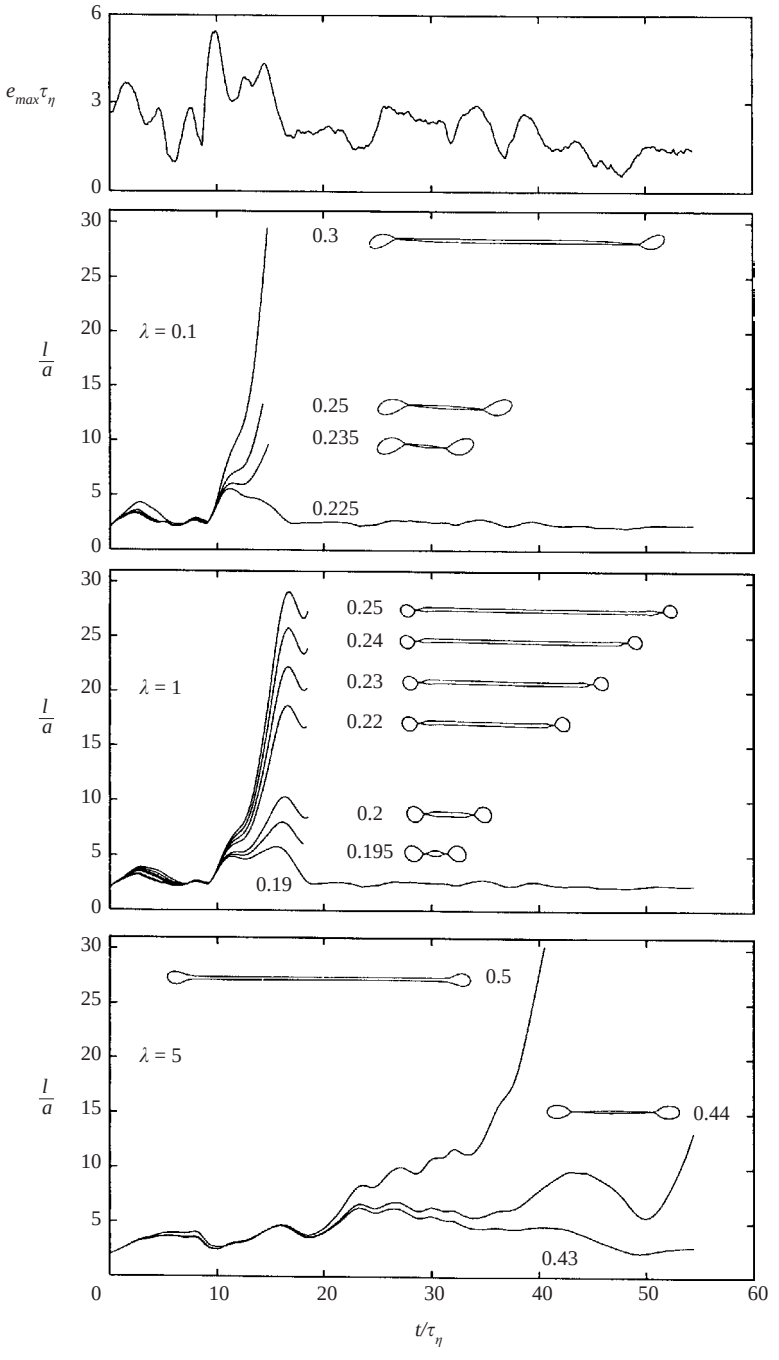

FIGURE 4. Evolution of drop length and flow strength with $\lambda = 0.1, 1, 5$ and $\bar{v}^{1/3}$ as labelled; drop shapes at the onset of pinch-off are shown.

reliable predictions, provided that the drop size parameter was adjusted (up to 15%). An example is shown in figure 2 (dashed-curve).

We have not been able to develop a simplified model for the drop orientation $\hat{\boldsymbol{l}}(t)$, given the time-dependent ambient flow. According to our simulations, the evolution

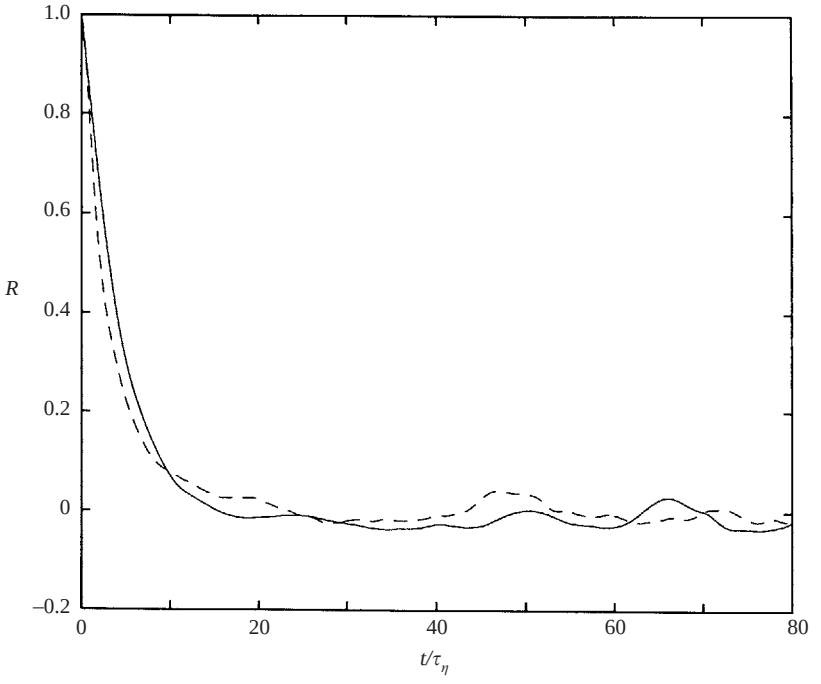

FIGURE 5. Autocorrelations of drop length (solid curve) and flow strength (dashed curve), $\bar{v}^{1/3} = 0.3,\ \lambda = 1$.

of drop orientation is qualitatively distinct from the evolution of a passive material element, except in the strong-flow limit (i.e. rapid breakup conditions), where drop shapes resemble slender filaments (Tjahjadi & Ottino 1991). As shown in § 5.2, drop deformation, rather than drop rotation, is the dominant mechanism for drop reorientation under small- and moderate-deformation conditions.

5. Statistical analysis

5.1. *Correlation times*

A statistical analysis of the system was performed for the case $\lambda = 1$. Simulation times much longer than the correlation time for the drop dynamics were used to ensure that the results presented below represent the stationary behaviour of the system.

Time autocorrelation functions for flow-strength e_{max} and drop length l, calculated for $\bar{v}^{1/3} = 0.3$, are shown in figure 5. The autocorrelation $R_Q(t)$ of the quantity $Q(t)$, where $Q = e_{max}$ or $Q = l$, was evaluated from an ensemble of 100 trajectories, each corresponding to an elapsed time $t_0 = 136\tau_\eta$. Broken drops were discarded from the ensemble at the time of pinch-off t_b (for $\bar{v}^{1/3} = 0.3$, breakup occurred on 36 trajectories). The autocorrelation functions were calculated using both ensemble and time averaging,

$$R_Q(t) = \frac{\left\langle \int_0^T \Delta Q(t')\ \Delta Q(t'+t)\,\mathrm{d}t' \right\rangle}{\left\langle \int_0^T \Delta Q(t')^2\,\mathrm{d}t' \right\rangle}, \tag{5.1}$$

where $\Delta Q(t) = Q(t) - \langle Q(t) \rangle$, $T = \min(t_0, t_b)$, and $\langle \ldots \rangle$ denotes the ensemble average.

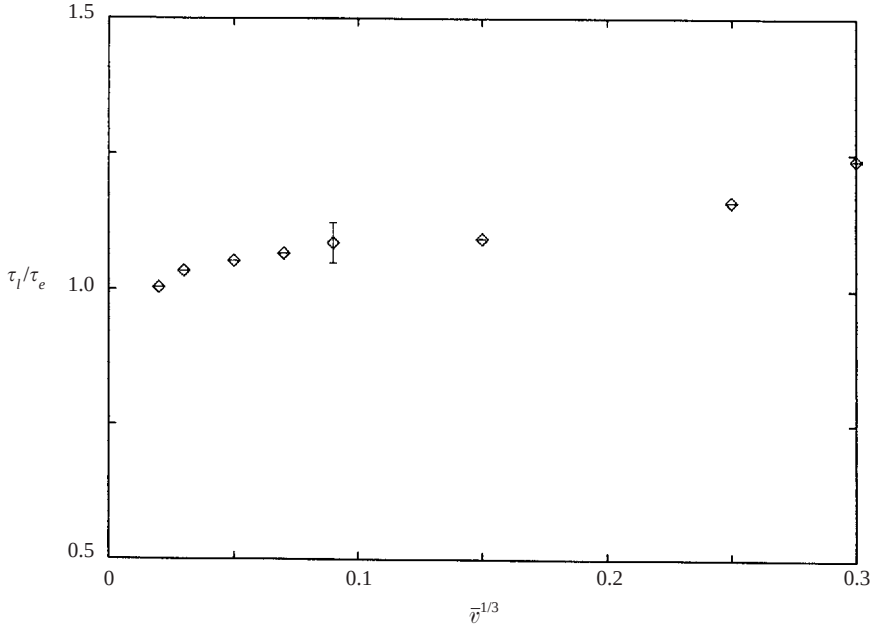

FIGURE 6. Drop-length correlation time versus drop size parameter, $\lambda = 1$. A representative error bar is shown.

The corresponding correlation time is defined as

$$\tau_Q = \int_0^\infty R_Q(t')\,\mathrm{d}t. \tag{5.2}$$

In our simulations, the calculated flow-strength correlation time was

$$\tau_e/\tau_\eta \simeq 2.4, \tag{5.3}$$

in agreement with the measurements of Pope (1990). According to the results shown in figure 6, $\tau_l \approx \tau_e$, consistent with the rapid response of low- and moderate-viscosity drops to fluctuations in flow strength, seen in figure 4. Drop dynamics are quasi-static in the limit $\tau_\sigma/\tau_\eta \to 0$ (discussed below), thus $\lim_{\bar{v}\to 0} \tau_l = \tau_e$.

5.2. *Distributions of drop length and orientation*

The cumulative probability distributions P for drop length and drop orientation, shown in figure 7, were calculated by time-averaging the instantaneous distributions from the ensemble of drop trajectories described above.

Drop orientation with respect to the local velocity field is characterized by the parameter

$$\beta(\hat{\boldsymbol{l}}) = \frac{e_l}{\|\mathbf{e}\|}, \tag{5.4}$$

where e_l is the projection (4.1), and $\|\mathbf{e}\| = (\mathbf{e}:\mathbf{e})^{1/2}$ ($\beta = 1$ corresponds to $\hat{\boldsymbol{l}}$ parallel to the z-axis in axisymmetric straining flow (4.3)). On a given trajectory, maximum drop alignment (i.e. maximum value of β) corresponds to

$$\hat{\boldsymbol{l}} = \hat{\boldsymbol{e}}_{max}, \tag{5.5}$$

where $\hat{\boldsymbol{e}}_{max}$ is the eigenvector associated with the maximum eigenvalue, e_{max}.

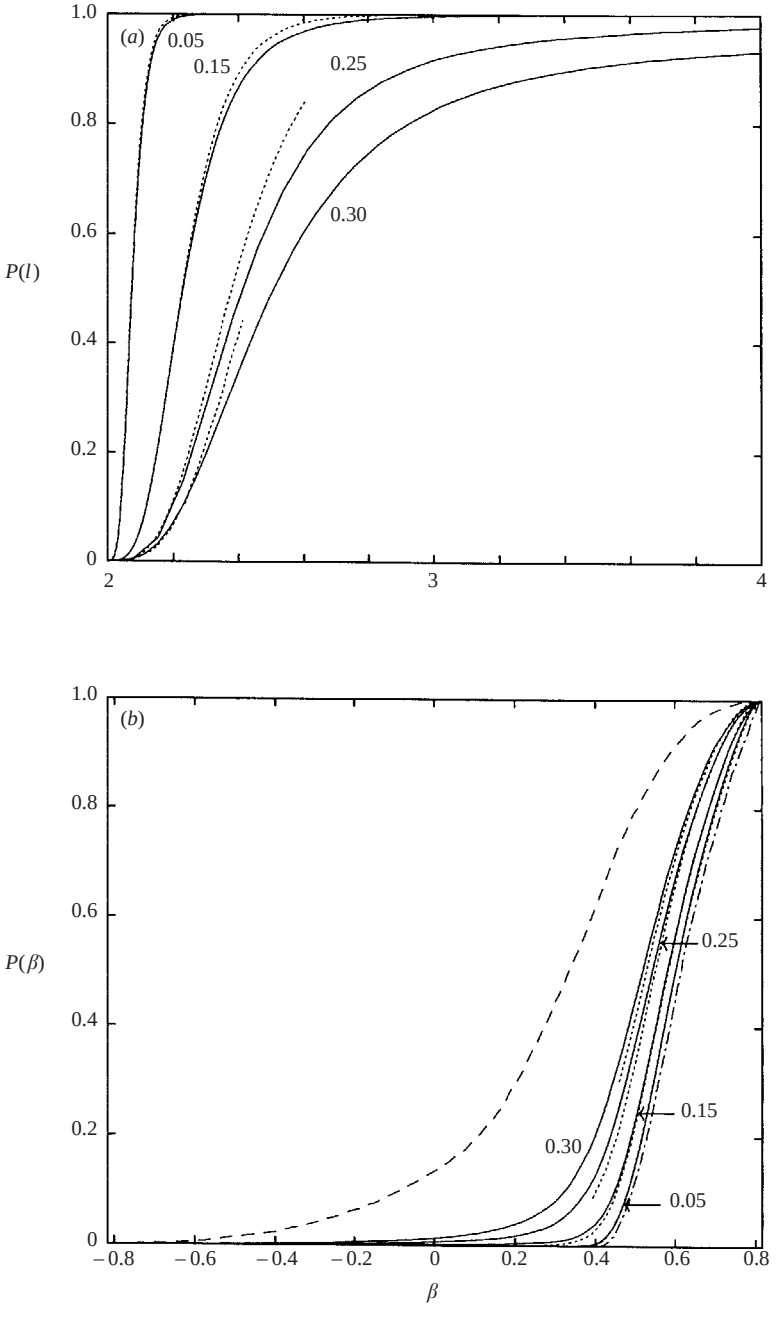

FIGURE 7. Stationary cumulative distributions of (a) drop length and (b) orientation parameter (5.4), $\lambda = 1$, $\bar{v}^{1/3} = 0.05, 0.15, 0.25, 0.30$ as labelled; numerical simulations (solid curves), $O(\bar{v})$ small deformation theory (dotted curves). Maximum alignment (5.5), $\bar{v} = 0$ (dashed-dotted curve), and orientation of material element (dashed curve) shown in (b).

In the small-deformation-limit $\bar{v}^{1/3} \to 0$, the drop-shape evolution is quasistatic because the capillary relaxation time is much less than the Kolmogorov time, according to equation (2.3). Under these conditions, the drop shape is described by $\xi/a = 1 + \bar{v}^{1/3}(\boldsymbol{C} : \hat{\boldsymbol{e}}_\xi \hat{\boldsymbol{e}}_\xi)$, where ξ is the distance of the drop interface from the drop

centre along the direction of the radial unit vector $\hat{\boldsymbol{e}}_\xi$, and $\boldsymbol{C}$ is the shape tensor

$$\boldsymbol{C}(t) = \frac{b_0}{b_1}\tau_\eta \mathbf{e}(t), \tag{5.6}$$

with $b_0 = 5/(2\lambda+3)$ and $b_1 = 8b_0(\lambda+1)/(19\lambda+16)$ (Leal 1992). This result indicates that maximum drop alignment (5.5) is achieved in the small-deformation limit. Under small-deformation-conditions $\tau_\sigma \ll \tau_\eta$, drop reorientation occurs quickly by deformation of the drop interface on the timescale τ_σ, rather than by rotation of the drop on the longer timescale τ_η.

The dashed-dotted curve in figure 7(*b*) shows the quasistatic prediction (5.5) for the cumulative distribution of drop orientation. The dotted curves in figure 7 show the predictions of an $O(\bar{v})$ perturbation expansion (Barthés-Biesel & Acrivos 1973). The drop-length distributions shown in figure 7(*a*) indicate that small-deformation-theory is accurate only for very modest deformations.

In the complementary strong-flow regime, elongated drop filaments reorient as passive material elements on the time scale τ_η. In our simulations, however, breakup events preclude large deformations. As a result, the drop orientation distributions shown in figure 7(*b*) are qualitatively distinct from the distribution corresponding to material elements (dashed curve); in fact, the drop orientation distributions are closer to maximum alignment (5.5).

The evolution of the conditionally averaged drop length and orientation prior to breakup events, shown in figure 8, were calculated from an ensemble of 36 trajectories corresponding to $\bar{v}^{1/3} = 0.3$. Large fluctuations result from the small size of the ensemble and the absence of time-averaging. The results show that after encountering the breaking fluctuation at $t_b - t \approx 10\tau_\eta$, drops elongate and misalign with respect to the flow, similar to a material element, in contrast to the near-maximum average alignment shown in figure 7(*b*). These results suggest that drop deformation, rather than rotation by the flow, is the dominant mechanism of drop reorientation in time-dependent flows with $\lambda \lesssim 1$, except immediately prior to breakup events.

5.3. *Breakup rates*

Our calculation of drop breakup rates is based on the assumption that the turbulent flow field along a drop trajectory can be represented by a sequence of uncorrelated fluctuations in the magnitude of the local strain rate. According to this picture, fluctuations are separated by intervals of relatively weak flow in which drop breakup does not occur. The strength of each fluctuation is characterized by a critical drop volume $\bar{v}^*$, such that drops with $\bar{v} > \bar{v}^*$ break in the fluctuation, and drops with $\bar{v} < \bar{v}^*$ do not break. The fluctuations are uncorrelated, provided that the time interval between them is large compared to the drop-length correlation time τ_l.

The distribution of the flow-field fluctuations is characterized by the fluctuation rate $f(\bar{v}^*)$, where $f(\bar{v}^*)\,\mathrm{d}\bar{v}^*$ represents the number per unit time of fluctuations with strength in the range $(\bar{v}^*, \bar{v}^* + \mathrm{d}\bar{v}^*)$. Under the assumptions of uncorrelated fluctuations and statistical equivalence of drop trajectories, drop breakup rates are given by the cumulative distribution of the flow-strength fluctuation frequency,

$$r(\bar{v}) = \int_0^{\bar{v}} f(s)\,\mathrm{d}s. \tag{5.7}$$

For uncorrelated fluctuations, this procedure is equivalent to computing $r(\bar{v})$ by determining the number of breakup events in a given time interval from simulations with $\bar{v}$ fixed. However, our approach is more efficient because separate simulations

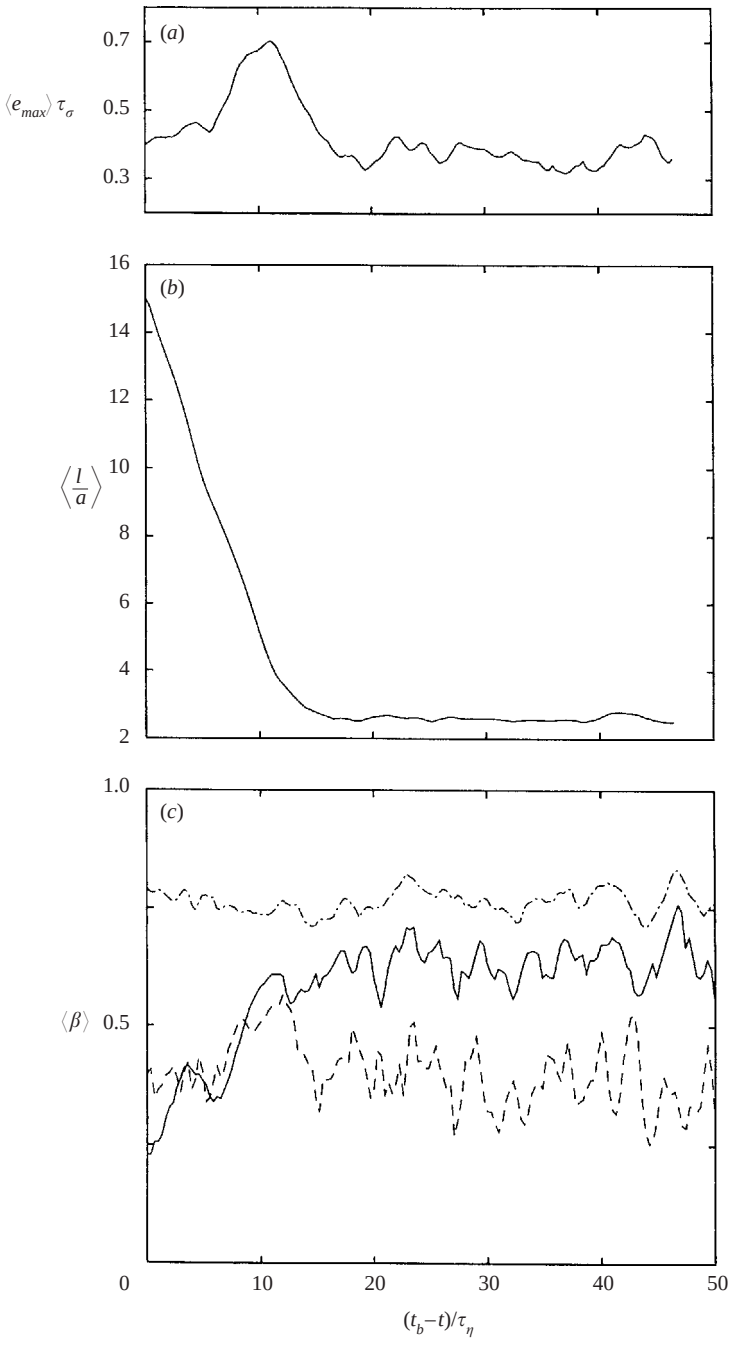

FIGURE 8. Evolution of average (*a*) flow strength, (*b*) drop length, and (*c*) orientation parameter (5.4) (solid curve) for trajectories resulting in drop breakup, $\bar{v}^{1/3} = 0.3$, $\lambda = 1$. Pinch-off occurs at $t = t_b$. Maximum alignment (5.5) (dashed-dotted curve) and orientation of material element (dashed curve) are shown in (*c*).

for each value of the drop size parameter are not required. Our approach is particularly useful in the long-time regime $\bar{v} \to 0$ associated with rare breakup events (cf. § 5.7).

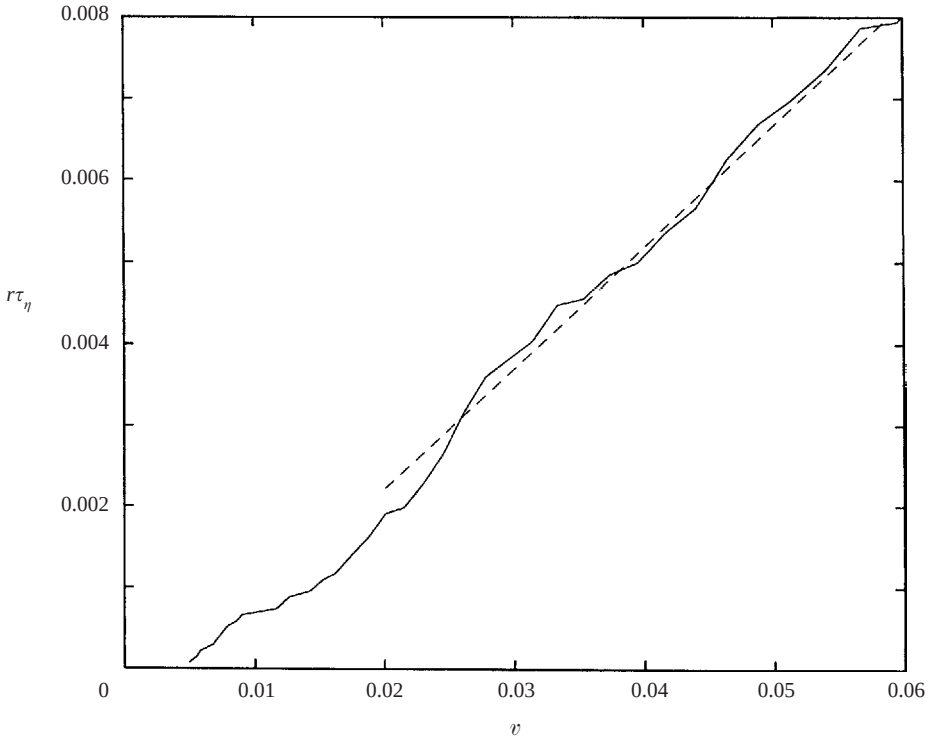

FIGURE 9. Breakup rates defined by (5.7), $\lambda = 1$ (solid curve); linear fit (5.8) (dashed curve).

The breakup rates shown in figure 9 were computed using formula (5.7) from an ensemble of 108 uncorrelated fluctuations with $\bar{v}^* \leqslant 0.06$, found within a total flow time $T_{tot} = 13,600\tau_\eta$. The upper limit ensures that the fluctuations were in fact uncorrelated. According to figure 6 and equation (5.3), the drop-length correlation time lies in the range $2.4\tau_\eta \leqslant \tau_l \lesssim 3.3\tau_\eta$, whereas the fluctuations in our simulations were isolated by at least $10\tau_\eta$. For each fluctuation, the critical drop size was evaluated from a series of boundary-integral simulations. For moderate drop volumes ($\bar{v} > 0.02$), our numerical results indicate that breakup rates are approximately described by the linear relation

$$r \approx k\bar{v}, \tag{5.8}$$

where $k\tau_\eta = 0.148 \pm 0.015$. An estimate of the relative statistical error in the rate calculation, based on the variance for a Poisson distribution, is $(r\,T_{tot})^{-1/2}$. Accordingly, breakup rates corresponding to the strongest fluctuations ($\bar{v} < 0.01$) are poorly resolved; longer simulations are required to resolve breakup rates for $\bar{v} \to 0$.

The same ensemble of flow fluctuations was used to evaluate the cummulative distribution $P(l^*)$ of critical drop lengths l^* (maximum drop length attained in a fluctuation without breakup). The broad critical drop-length distribution, seen in figure 10, implies that a finite fraction of drops become highly elongated without breakup (cf. example in figure 3). In contrast, drops in stationary Stokes flows have comparatively short critical lengths, (e.g. $l^*/a \approx 4.7$ in simple shear flow for $\lambda = 1$ (Bławzdziewicz, Cristini & Loewenberg 2002). Given that large deformations may occur without breakup, and that small deformation theory is reliable only for very modest deformations (cf. figure 7*a*), small deformation theory (or any description

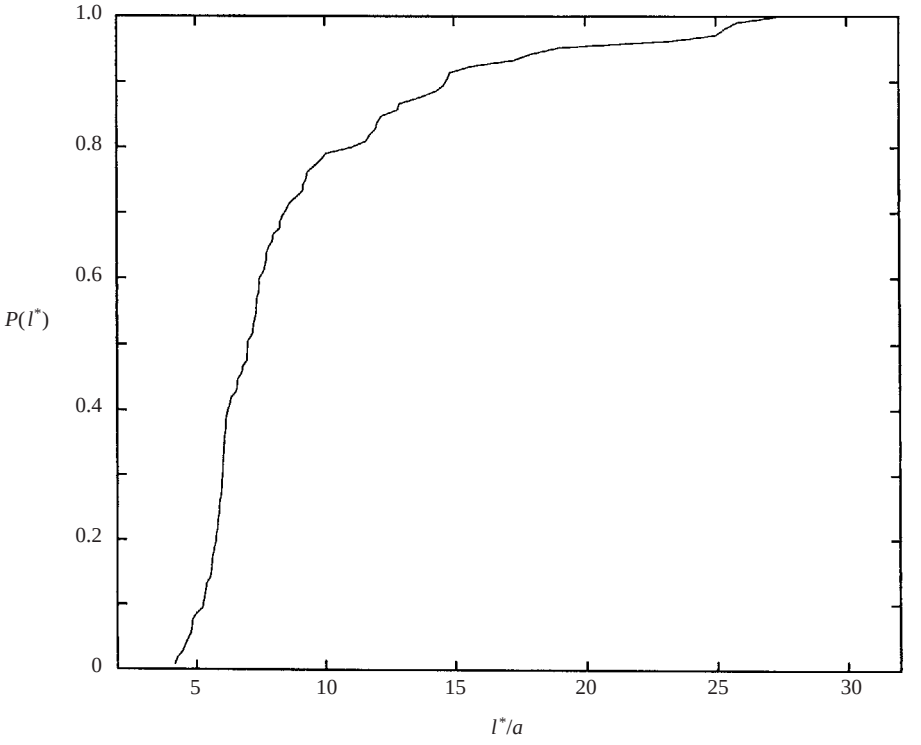

FIGURE 10. Cumulative distribution of critical drop length, $\lambda = 1$.

of drop dynamics which does not resolve the evolution of the neck) cannot reliably predict breakup events in time-dependent Stokes flows.

5.4. *Distribution of daughter drops*

The distribution of primary daughter-drop volumes, shown in figure 11, was computed from a simulations of 46 breakup events with $\lambda = 1$ and $0.18 \leqslant \bar{v}^{1/3} \leqslant 0.27$. The results are presented in a rescaled form, where each daughter-drop volume $\bar{v}_d$ is normalized by the corresponding critical drop size $\bar{v}^*$ for the fluctuation in which the breakup event occurs. Our simulation results show that this rescaling yields a narrow drop-size distribution with a mean value

$$\bar{v}_d/\bar{v}^* \approx b^{-1}, \tag{5.9}$$

where $b \approx 2$ is a partitioning constant.

The scaling (5.9) reflects the stress balance on the drop interface. The radius of curvature of a drop fragment (i.e. daughter-drop radius a_d) is determined by the balance between capillary and viscous stresses $\sigma/a_d \sim \mu\dot{\gamma}'$, where $\dot{\gamma}'$ is the characteristic strain rate for the fluctuation that breaks the drop. Accordingly, the daughter drop volume is given by

$$\bar{v}_d \sim (\tau_\eta \dot{\gamma}')^{-3}, \tag{5.10}$$

which is independent of the parent-drop volume. For $\bar{v} \approx \bar{v}^*$, breakup events produce two daughter drops with volume $\bar{v}_d \approx \bar{v}^*/2$. Thus, by the insensitivity with respect to parent-drop volume, equation (5.9) follows.

A similar scaling has been observed in experimental and numerical studies of drop breakup in simple shear flow under Stokes flow conditions (Marks 1998; Cristini *et al.*

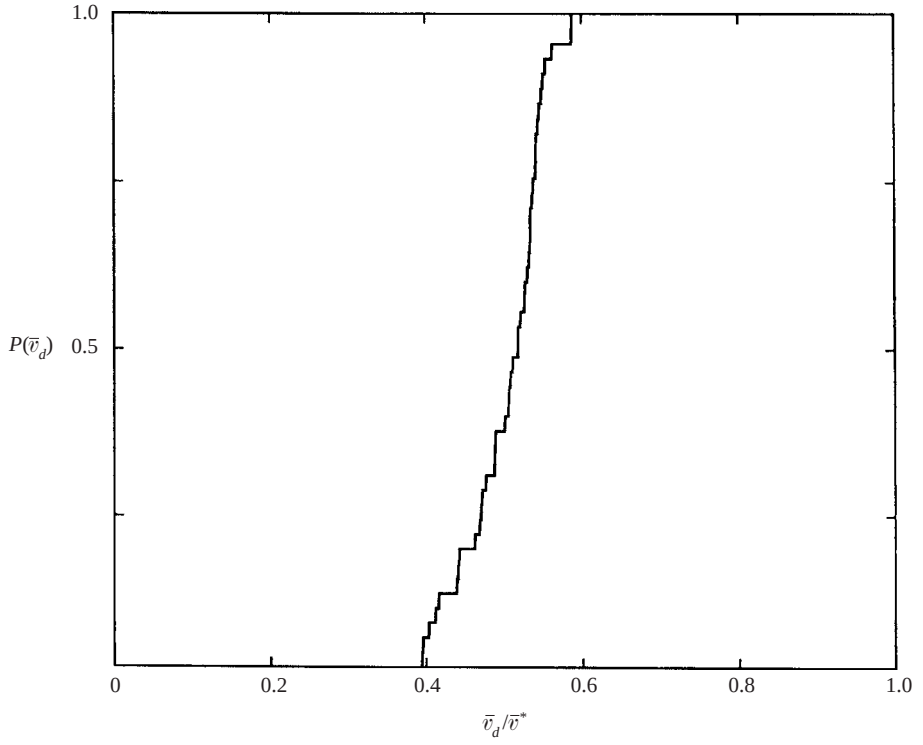

FIGURE 11. Cumulative distribution of daughter-drop volumes, $\lambda = 1$.

2003), and in simple shear with inertia (Renardy & Cristini 2001; Renardy, Cristini & Li 2002). This result contradicts the assumption, embedded in almost all models of drop breakup in a turbulent flow, that the daughter-drop-size distribution scales with the size of the parent drop (Lasheras *et al.* 2002; Sathyagal *et al.* 1996; Ramkrishna 2000).

5.5. *Evolution of the drop-size distribution*

Assuming that drop breakup events are uncorrelated and that drops do not coalesce, the evolution of the number density of drops $n(\bar{v}, t)$ of size $\bar{v}$ is governed by the population balance equation

$$\frac{\partial}{\partial t} n(\bar{v}, t) = \int_{\bar{v}}^{\infty} g(\bar{v}, \bar{v}') n(\bar{v}', t)\, \mathrm{d}\bar{v}' - r(\bar{v}) n(\bar{v}, t), \tag{5.11}$$

where $r(\bar{v})$ is the drop breakup rate (5.7), and $g(\bar{v}, \bar{v}')$ is the production rate of drops with volume $\bar{v}$ by the breakup of drops with volume $\bar{v}'$.

Because of its computational cost, it is impractical to evaluate the two-variable production-rate function $g(\bar{v}, \bar{v}')$ directly from boundary-integral simulations without resorting to some simplifications. Small deformation theory cannot be used to predict breakup rates, and the axisymmetric approximation (4.3) requires a model for predicting drop orientation. However, a simple approximation for $g(\bar{v}, \bar{v}')$ can be derived from estimate (5.9).

According to this estimate, the production rate $g_d(\bar{v}, \bar{v}')$ of primary daughter drops with volume $\bar{v}$ is approximately independent of the parent-drop volume $\bar{v}'$ and is

proportional to the fluctuation strength, characterized by $\bar{v}^*$. Thus, we have

$$g_d(\bar{v}, \bar{v}') \approx 2bf(b\bar{v}), \tag{5.12}$$

where the factor b on the right-hand side results from the change of variables between $\bar{v}$ and $\bar{v}^* = b\bar{v}$ in the fluctuation-strength frequency.

Approximation (5.12) leads to the simplified evolution equation for the primary drop fragments produced by breakup events

$$\frac{\partial}{\partial t} n(\bar{v}, t) = 2bf(b\bar{v}) \int_{b\bar{v}}^{\infty} n(\bar{v}', t)\, \mathrm{d}\bar{v}' - n(\bar{v}, t) \int_0^{\bar{v}} f(\bar{v}')\, \mathrm{d}\bar{v}', \tag{5.13}$$

which is obtained from (5.11) by replacing $g(\bar{v}, \bar{v}')$ with $g_d(\bar{v}, \bar{v}')$. In equation (5.13), the excess volume $\bar{v}' - 2\bar{v}$ that is partitioned into smaller satellite drops is neglected, because secondary breakup events leading to the formation to such satellites were not resolved in our simulations. A more detailed description, where the distribution of satellite drops is also modelled, will be discussed in a separate publication.

5.6. *Moments of the drop size distribution*

In this section, we derive an analytical solution of the evolution equation (5.13) with a power-law breakup rate

$$r = k\bar{v}^q, \tag{5.14}$$

and a monodisperse initial drop-size distribution

$$n(\bar{v}, 0) = \delta(\bar{v} - \bar{v}_0) n_0, \tag{5.15}$$

where n_0 is the initial number density of drops, and $\bar{v}_0$ is the initial drop volume. The results for an arbitrary initial condition can be obtained by linear superposition.

Multiplying equation (5.13) by $\bar{v}^i$ and integrating with respect to $\bar{v}$ yields

$$M_i'(t) = -k \left(1 - \frac{2qb^{-i}}{i+q}\right) M_{i+q}(t), \tag{5.16}$$

where

$$M_i(t) = \int_0^{\infty} \bar{v}^i n(\bar{v}, t)\, \mathrm{d}\bar{v}, \qquad i = 0, 1, 2 \ldots \tag{5.17}$$

are moments of the drop size distribution, and $M_i'(t)$ denotes a time derivative of $M_i(t)$. Higher-order time derivatives of the moments are obtained by iterative application of (5.16)

$$M_i^{(p)}(t) = (-k)^p \prod_{j=1}^{p} \left(1 - \frac{2qb^{-i-(j-1)q}}{i+jq}\right) M_{i+pq}(t), \tag{5.18}$$

where $p = 1, 2, \ldots$ According to initial condition (5.15),

$$M_i(0) = n_0 \bar{v}_0^i. \tag{5.19}$$

Thus, equation (5.18) can be used to generate the Taylor series expansion for the normalized moments $\bar{M}_i(t) = M_i(t)/M_i(0)$

$$\bar{M}_i(t) = \sum_{p=0}^{\infty} \frac{(-\bar{k}t)^p}{p!} \prod_{j=1}^{p} \left(1 - \frac{2qb^{-i-(j-1)q}}{i+jq}\right), \tag{5.20}$$

where $\bar{k} = k\bar{v}_0^q$.

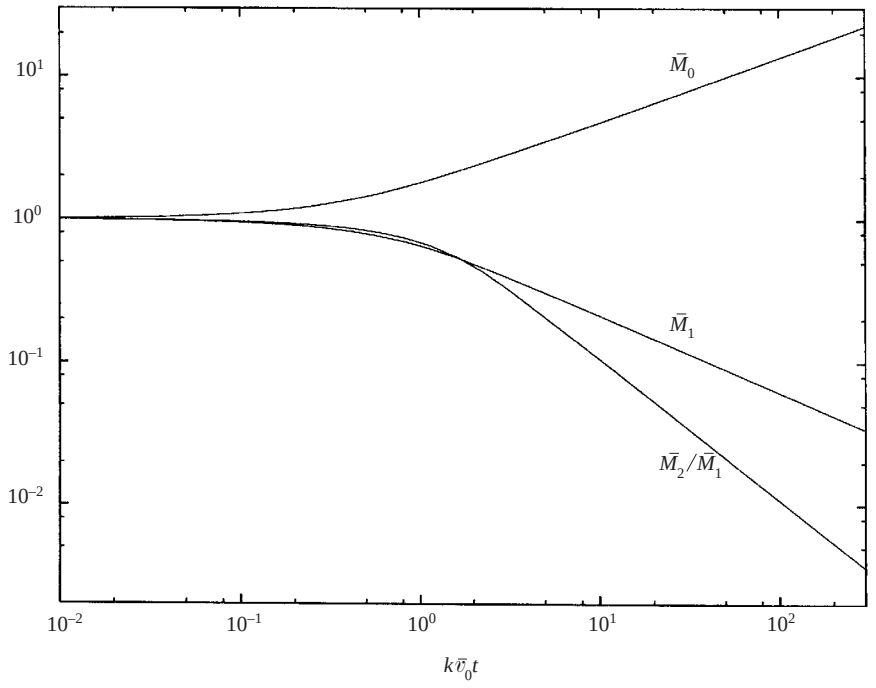

FIGURE 12. Evolution of moments of drop size distribution (5.20) corresponding to breakup rate (5.8) and partitioning constant $b = 2$.

Solution (5.20) is shown in figure 12 for a system with a linear breakup rate, $q = 1$, and partitioning constant $b = 2$. These parameter values are consistent with our simulations (cf. equation (5.8) and figure 11). The curves in figure 12 correspond to the drop number density $\bar{M}_0$, the total drop volume $\bar{M}_1$, and the average drop volume $\bar{M}_2/\bar{M}_1$. The total volume of primary daughter drops $\bar{M}_1$ decays with time, because satellite drops produced by secondary breakup events are not included in the evolution equation (5.13). The results reveal an algebraic evolution of the moments at long times.

5.7. *The role of rare events*

Since only small drops survive at long times, rare strong fluctuations are required for further breakup. According to the multifractal theory of turbulent intermittency, fluctuations in the energy dissipation rate ϵ' scale as (Frisch 1995)

$$\epsilon'/\epsilon \sim (s'/L)^{\alpha-1}, \tag{5.21}$$

for $Re_L \to \infty$, where L is the integral lengthscale, s' is the lengthscale associated with the fluctuation, $Re_L = (L/\eta)^{4/3}$ is the integral-scale Reynolds number, and α is the singularity exponent. Assuming $\alpha \approx 0$, corresponding to the strongest fluctuations (Meneveau & Sreenivasan 1991), and taking $s' \approx \eta' \equiv \nu^{3/4}\epsilon'^{-1/4}$, we obtain

$$\epsilon'/\epsilon \sim Re_L. \tag{5.22}$$

An estimate for the corresponding critical drop size parameter at high Reynolds numbers is obtained by inserting the characteristic shear rate $\dot{\gamma}' = \nu/\eta'^2$ into equation (5.10)

$$\bar{v}^* \sim Re_L^{-3/2}. \tag{5.23}$$

Accordingly, equation (2.4) becomes

$$a/\eta' \sim \left(\mu^{-5/4}\sigma\rho^{1/4}\epsilon^{-1/4}\right) Re_L^{-1/4}. \tag{5.24}$$

The additional factor $Re_L^{-1/4}$ suggests that the sub-Kolmogorov regime considered in this study has broader relevance at high Reynolds numbers and long times.

Testing the predicted Reynolds-number dependence (5.23) with numerical simulations will require longer simulation times and a range of larger Reynolds numbers. Recent simulations of isotropic turbulence at Reynolds numbers up to 234 (based on the Taylor microscale) show evidence of intermittency (Yeung 2001). The computational strategy developed in our study is particularly efficient for computer simulations of drop dynamics in the long-time regime. Accordingly, an ensemble of isolated strong fluctuations is obtained by applying a flow-strength criterion or a simplified model of the drop dynamics. Boundary-integral simulations are only required for computing the critical drop size for each fluctuation, and breakup rates are given by the cummulative distribution of critical drop sizes.

J. B., V. C., and M. L. were supported by NSF grant CTS-9624615 and NASA grant NAG3-2477; V. C. had additional support from an NSF grant; L. R. C. was supported by NSF grant CTS-9417527 and NASA grant NAG3-270.

REFERENCES

Barthés-Biesel, D. & Acrivos, A. 1973 Deformation and burst of a liquid droplet freely suspended in a linear shear field. *J. Fluid Mech.* **61**, 1–21.

Bławzdziewicz, J., Cristini, V. & Loewenberg, M. 1997 Analysis of drop breakup in creeping flows. *Bull. Am. Phys. Soc.* **42**, 2125.

Bławzdziewicz, J., Cristini, V. & Loewenberg, M. 2002 Critical behavior of drops in linear flows: I. phenomenological theory for drop dynamics near critical stationary states. *Phys. Fluids* **14**, 2709–2718.

Canuto, C., Hussaini, M. Y., Quarteroni, A. & Zang, T. A. 1988 *Spectral Methods in Fluid Dynamics*. Springer.

Coulaloglou, C. A. & Tavlarides, L. L. 1977 Description of the interaction processes in agitated liquid–liquid dispersions. *AICHE J.* **32**, 1287–1297.

Cristini, V., Bławzdziewicz, J. & Loewenberg, M. 2001 An adaptive mesh algorithm for evolving surfaces: simulations of drop breakup and coalescence. *Comput. Phys.* **168**, 445–463.

Cristini, V., Bławzdziewicz, J., Loewenberg, M., Guido, S. & Alfani, A. 2003 Drop breakup and fragment size distribution in shear flow. *J. Rheol.* **47** (to appear).

Eswaran, V. & Pope, S. B. 1988 An examination of forcing in direct numerical simulations of turbulence. *Comput. Fluids* **16**, 257.

Frisch, U. 1995 *Turbulence*. Cambridge University Press.

Hinze, O. 1955 Fundamentals of the hydrodynamic mechanism of splitting in dispersion processes. *AICHE J.* **1**, 289–295.

Kolmogorov, A. N. 1949 On the disintegration of drops in turbulent flow. *Dokl. Akad. Nauk.* **66**, 825–828.

Lasheras, J. C., Eastwood, C., Martínez-Bazán, C. & Montanes, J. L. 2002 A review of statistical models for the break-up of an immiscible fluid immersed into a fully developed turbulent flow. *Intl J. Multiphase Flow* **28**, 247–278.

Leal, L. 1992 *Laminar Flow and Convective Transport Processes*. Butterworth–Heinemann.

Lister, J. R. & Stone, H. A. 1998 Capillary breakup of a viscous thread surrounded by another viscous fluid. *Phys. Fluids* **10**, 2758–2764.

Marks, C. 1998 Drop breakup and deformation in sudden onset strong flows. PhD thesis, University Maryland, College Park.

Meneveau, C. & Sreenivasan, K. R. 1991 Multifractal nature of turbulent energy dissipation. *J. Fluid Mech.* **224**, 429–484.

Patel, P., Shaqfeh, E., Butler, J., Cristini, V., Blawzdziewicz, J. & Loewenberg, M. 2003 Drop breakup in the flow through fixed fiber beds: an experimental and computational investigation. *Phys. Fluids* **15**, 1146–1157.

Pope, S. B. 1990 Lagrangian microscales in turbulence. *Phil. Trans. R. Soc. Lond.* A **333**, 309–319.

Pozrikidis, C. 1992 *Boundary Integral and Singularity Methods for Linearized Viscous Flow*. Cambridge University Press.

Ramkrishna, D. 2000 *Population Balances: Theory and Applications to Particulate Systems in Engineering*. Academic.

Renardy, Y. & Cristini, V. 2001 Scalings for fragments produced from drop breakup in shear flow with inertia. *Phys. Fluids* **13**, 2161–2164.

Renardy, Y., Cristini, V. & Li, J. 2002 Drop fragment distributions under shear with inertia. *Intl J. Multiphase Flow* **28**, 1125–1147.

Sathyagal, A. N., Ramkrishna, D. & Narsimhan, G. 1996 Droplet breakage in stirred dispersions. Breakage functions from experimental drop-size distributions. *Chem. Engng Sci.* **51**, 1377–1391.

Shreekumar, Kumar, R. & Gandhi, K. S. 1996 Breakage of a drop of inviscid fluid due to a pressure fluctuation at its surface. *J. Fluid Mech.* **328**, 1–17.

Sundaram, S. & Collins, L. R. 1997 Collision statistics in an isotropic, particle-laden turbulent suspension I. direct numerical simulations. *J. Fluid Mech.* **335**, 75–109.

Tjahjadi, M. & Ottino, J. M. 1991 Stretching and breakup of droplets in chaotic flows. *J. Fluid Mech.* **232**, 191–219.

Tsouris, C. & Tavlarides, L. L. 1994 Breakage and coalescence models for drops in turbulent dispersions. *AICHE J.* **40**, 395–406.

Yeung, P. K. 2001 Lagrangian characteristics of turbulence and scalar transport in direct numerical simulations. *J. Fluid Mech.* **427**, 241–274.